

Supporting information

From the Junkyard to the Power Grid: Ambient Processing of Scrap Metals into Nanostructured Electrodes for Ultrafast Rechargeable Batteries

*Nitin Muralidharan,^{1,2,‡} Andrew S. Westover,^{1,2,‡} Haotian Sun,² Nicholas Galioto,² Rachel E. Carter,²
Adam P. Cohn,² Landon Oakes^{1,2} and Cary L. Pint^{1,2*}*

¹Interdisciplinary Materials Science Program, Vanderbilt University, Nashville, TN 37235

²Department of Mechanical Engineering, Vanderbilt University, Nashville TN 37235

[‡]These authors contributed equally to this work

*Corresponding author: cary.l.pint@vanderbilt.edu

Experimental Methods:

Development of iron oxide nanorods and copper oxide nanothorns

The obtained scrap carbon steel (1010 steel) and brass sheets (Yellow brass, 67% Cu/33% Zn) were cut into small squares and subjected to ultrasonic cleaning using acetone, ethanol and water for 10 min each. For the preparation of iron oxide nanorods, the steel samples were subjected to potentiostatic anodization at 40 V for 900 seconds using a Keithley sourcemeter. The electrolyte used in this case contained 0.05M NH_4F in 3 vol% of water with ethylene glycol. The anodized steel samples were washed with water and dried in air. To stabilize the surface oxide, an annealing step was added where the sheets were subjected to a temperature of 350 °C for 1 hour under $\text{Ar}(1\text{SLM})/\text{H}_2(200\text{ sccm})$ flow. To prepare copper oxide nanothorns, the ultrasonically cleaned brass sheets were soaked in HCl where the initial solution (37%) HCl (sigma aldrich) was diluted down in a ratio of 10 mL of ultrapure water to 5 mL of 37% (HCl). This allowed for removal of the native oxide. Anodization was then performed in a 2M KOH electrolyte using 100 cyclic voltammetric sweeps between 0 V and 0.6 V using a Metrohm Autolab controller. To truly demonstrate the versatility of the anodization process, brass sheets were anodized galvanostatically as well using a current density of 1 mA/cm^2 for 300 seconds. The counter electrode and the reference electrode in these set ups were a Pt foil and saturated calomel electrode respectively. The anodized brass sheets were washed with water and dried in air. Similar anodization and post treatment conditions were followed for the scrap screws, pipes and trimmings.

In order to assess the active mass, the active materials on the surface were mechanically separated from the electrodes. This technique was compared to other techniques for active mass assessment including (1) the dissolution of active oxides in liquid media and corresponding mass

assessment, and (2) 3-D SEM profiles for active mass isolation. The mechanical separation approach, albeit very simple, errors on the side of overestimating the active mass due to the potential removal of some inactive material, providing an underestimate of the actual electrode performance. This is in comparison to dissolution processes which can error on the side of an underestimate for active mass, and similar for SEM analysis techniques. Thus mechanical separation was established as the best method for this work, and was used throughout the manuscript.

Microstructural and Compositional Analysis

Microstructural analysis and Energy Dispersive Spectroscopy (EDS) elemental analysis were performed on the anodized and treated steel and brass surfaces using a Zeiss Merlin Scanning Electron Microscope. Compositional analysis of the anodized brass and steel surfaces were also performed using Renishaw Raman Microscope using 532 nm Laser excitations to determine the surface species corresponding to the different nanostructures.

Electrochemical Characterization

The anodized steel and brass samples were subjected to electrochemical testing individually in a .1M or 1M KOH electrolyte with a Pt counter and SCE reference electrode in a beaker type electrochemical cell. For the scrap metal battery, the steel electrode was made the anode and the brass electrode the cathode, the electrolyte used was 1 M KOH. A jar type battery was made using the same electrode configuration in a glass vial sealed with a rubber septa forming a full cell. Two such jar batteries were connected in series to reach the required voltage to power a blue LED. The jar battery system was galvanostatically charged and then a blue LED was connected to the jar battery which allowed for the jar battery to discharge thereby lighting the LED. All electrochemical characterization was performed using a Metrohm Autolab

Multichannel Analyzer. All full cells were cycled a 100 CV cycles for conditioning and to obtain reproducible voltammograms.

Specific capacity was calculated from CV curves using the equation $Capacity_{sp} = \frac{\int I dV}{m \cdot dV/dt}$ and

from discharge curves using the equation $Capacity_{sp} = \frac{I \cdot t}{m}$. Specific Capacitance was calculated

from CV curves using the equation $Capacitance_{sp} = \frac{\int I dV}{V \cdot m \cdot dV/dt}$. In all cases I represents the

current, V is the voltage, m is the mass, and dV/dt is the scan rate. Specific energy was

calculated from the discharge curves according to the equation $Energy_{sp} = \frac{\int IV dt}{m}$ and the

specific power was calculated according to the following equation. $Power = \frac{Energy_{sp}}{\Delta t}$.

EDS compositional analysis:

Elemental mapping and analysis of the iron oxide nanorods using EDS

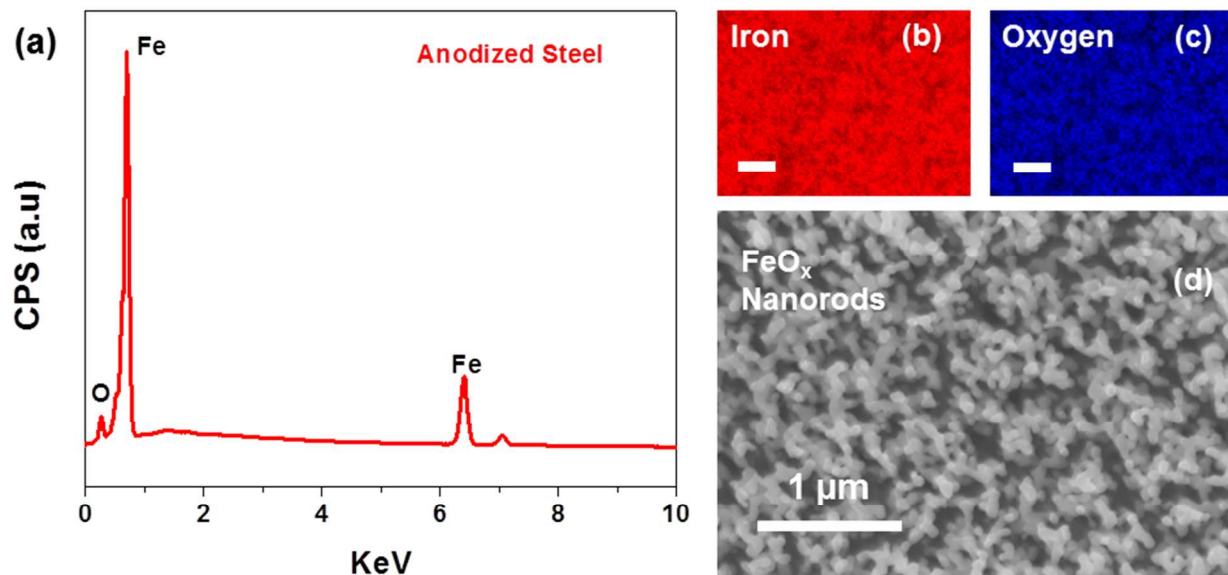


Figure S1. (a) Energy Dispersive Spectroscopy (EDS) spectra of the treated steel surface consisting of the FeO_x nanorods. (b) EDS map of the iron oxide nanorods showing the elemental signature of iron. (c) EDS map of the iron oxide nanorods showing the elemental signature of oxygen. (d) Electron image of the iron oxide nanorods.

Presence of surface oxides of iron forming the iron oxide nanorods are observed in the elemental analysis. This indicates that the surface treatments render the bare steel surface oxidized.

Elemental mapping and analysis of the copper oxide nanothorns using EDS

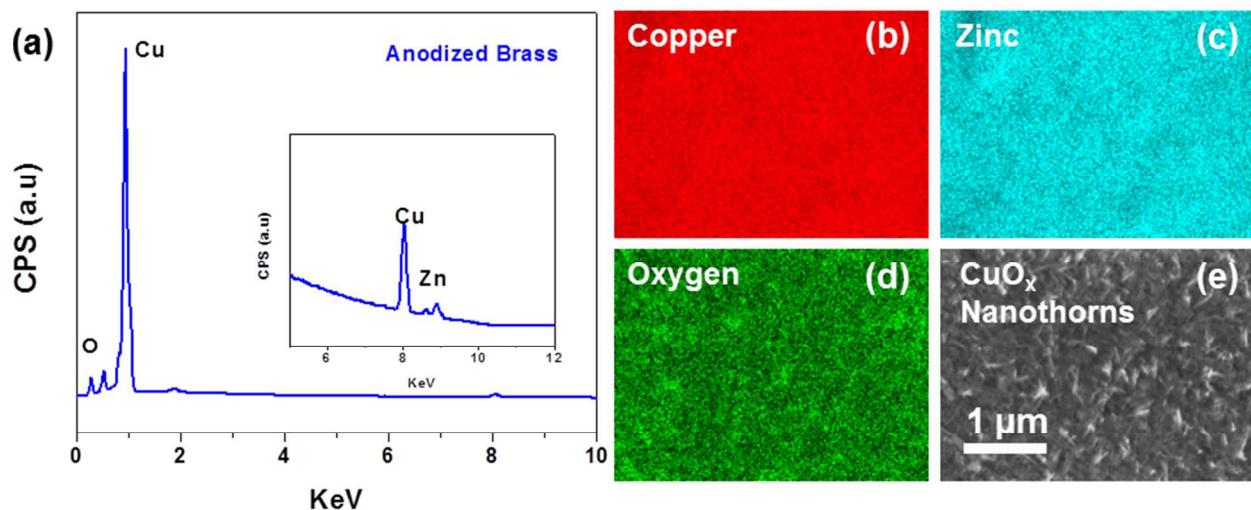


Figure S2. (a) Energy Dispersive Spectroscopy (EDS) spectra of the treated brass surface consisting of the CuO_x nanothorns, inset – EDS spectra between 5 and 12 KeV showing elemental signature of copper and zinc (b) EDS map of the copper oxide nanothorns showing the elemental signature of copper. (c) EDS map of the copper oxide nanothorns showing the elemental signature of zinc. (d) EDS map of the copper oxide nanothorns showing the elemental signature of oxygen. (e) Electron image of the copper oxide nanothorns.

EDS elemental analysis indicates the presence of copper, zinc and oxygen for the anodized brass surface indicating the presence of oxides of copper and zinc.

Educational Module: Classification of Batteries, Supercapacitors and Pseudocapacitors

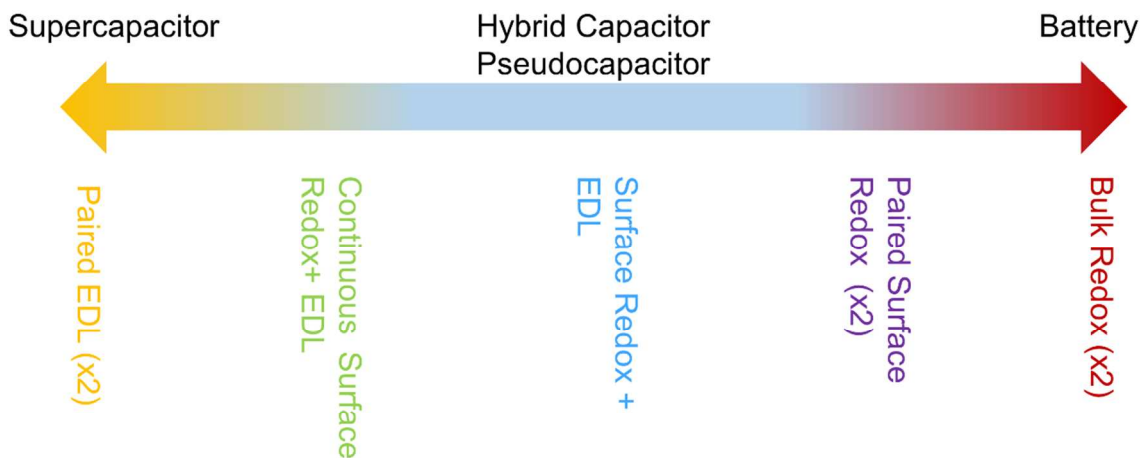


Figure S3. Schematic representation of the general classification of supercapacitors, batteries and hybrid devices

Electric double layer (EDL)	High Power	Low Energy	Electrostatic	CNT ¹ , AC, Graphene ²
Continuous Surface Redox	High Power	Moderate Energy	Faradaic	MnO ₂ , ³ RuO ₂ . ⁴
Surface Redox	High Power	Moderate Energy	Faradaic	NiOH, ⁵ Fe ₂ O ₃ , ⁶ Cu(OH) ₂ , Co ₂ O ₃ , ⁷ Nanoparticles
Bulk Redox	Low	High Energy	Faradaic	Zn ⁸ , Pb ⁹ , Ni ¹⁰ , LiCoO ₂ , ¹² Graphite, ¹¹

Table S4: Classification of the similarities and difference between different electrode types for energy storage

Historically, there has been considerable debate as to what exactly is the distinction between the different types of energy storage devices. Conventionally these have been split into three different categories Electric Double Layer Capacitors (EDLC), Pseudocapacitors, and Batteries. Where the terms Supercapacitor and ultracapacitor have often been used to describe

both EDLC and pseudocapacitors. The most comprehensive and possibly insightful description of these types of devices was given by Conway.¹³ He clearly described the distinction between each of the different types of energy storage electrodes. According to Conway there are essentially four different types of electrodes (see above Table S4). The first of these is electric double layer capacitors, where the energy is stored electrostatically by forming an ionic double layer on the surface of an electrode and except for a few exceptions consist almost entirely of carbon nanomaterials. The second is that of electrodes that exhibit a series of faradaic surface redox reactions such that in almost all respects their behavior mimics that of an EDLC with box-like CV curves and triangular charge discharge curves. The most common examples of these are MnO_2 and RuO_2 . The third type of electrode is similar to the surface redox reactions exhibited by the second, except whereas this second type of electrode exhibits a series of continuous chemical reactions causing the performance to mimic that of a traditional EDLC, this third type exhibit a much narrower range of faradaic reactions, often coming from a single chemical reaction. He distinguishes this third type of electrode from traditional faradaic battery electrodes in that the chemical reactions for the most part happen on the surface of the material and do not cause a permanent phase change in the bulk of the material. Finally the fourth type he describes is that of battery electrodes which rely on bulk chemical reactions that cause a complete phase change of the electrode material.

Although the classifications between the different types of electrodes is very clear, when pairing the devices together the definitions become more vague and less well defined. In particular for the electrodes that are traditionally classified as pseudocapacitor electrodes, just as for any redox reaction these electrodes cannot be paired with themselves and form a fully functioning energy storage device. The vast majority of full cell applications of these

‘pseudocapacitor’ electrodes have involved the pairing of them with traditional EDLC and for these hybrid devices classifying them as supercapacitors, hybrid supercapacitors, asymmetric supercapacitors or any variation of such which is extremely appropriate. Recently however there has been a new class of full cell devices that pair what sometimes are traditionally considered ‘pseudocapacitor’ electrodes in order to maximize the voltage separation and capacities in the same manner as that used for designing traditional batteries. For these devices in almost all respects the full cells behave like that of a battery, with distinct faradaic energy storage peaks in the CV curves and long plateaus in the charge and discharge curves. The one distinction between these materials and that of traditional batteries is that the energy storage is primarily on the surface leading to excellent energy performance in the high power regime which is normally dominated by supercapacitors and hybrid supercapacitor architectures. Authors of works describing these paired systems have commonly referred to them as ‘high rate batteries’, ‘ultrafast batteries’, and ‘ultrabatteries’. This is in accordance with the recently published works by Simon, Gogotsi and Dunn^{2, 14} that recommended that although these devices may exhibit high power it is still most appropriate to refer to these devices as batteries.¹⁵

Our electrodes clearly fall into this final type of full cell device, where we have the pairing of two electrodes that exhibit surface based redox reactions. In accordance with the guidelines outlined by Simon, Gogotsi, and Dunn where the device is characterized by the electrochemical behavior in both charge-discharge and CV measurements we refer to our devices as batteries. Because of the high rate performance of the devices, and due to the fact that each electrode could be individually paired with an EDLC to form a hybrid asymmetric supercapacitors we also feel strongly that the characterization of the performance of the individual electrodes should be characterized in terms of capacitance as well.”

Electrochemical Impedance Spectroscopy of the Scrap Metal Battery (Full Cell)

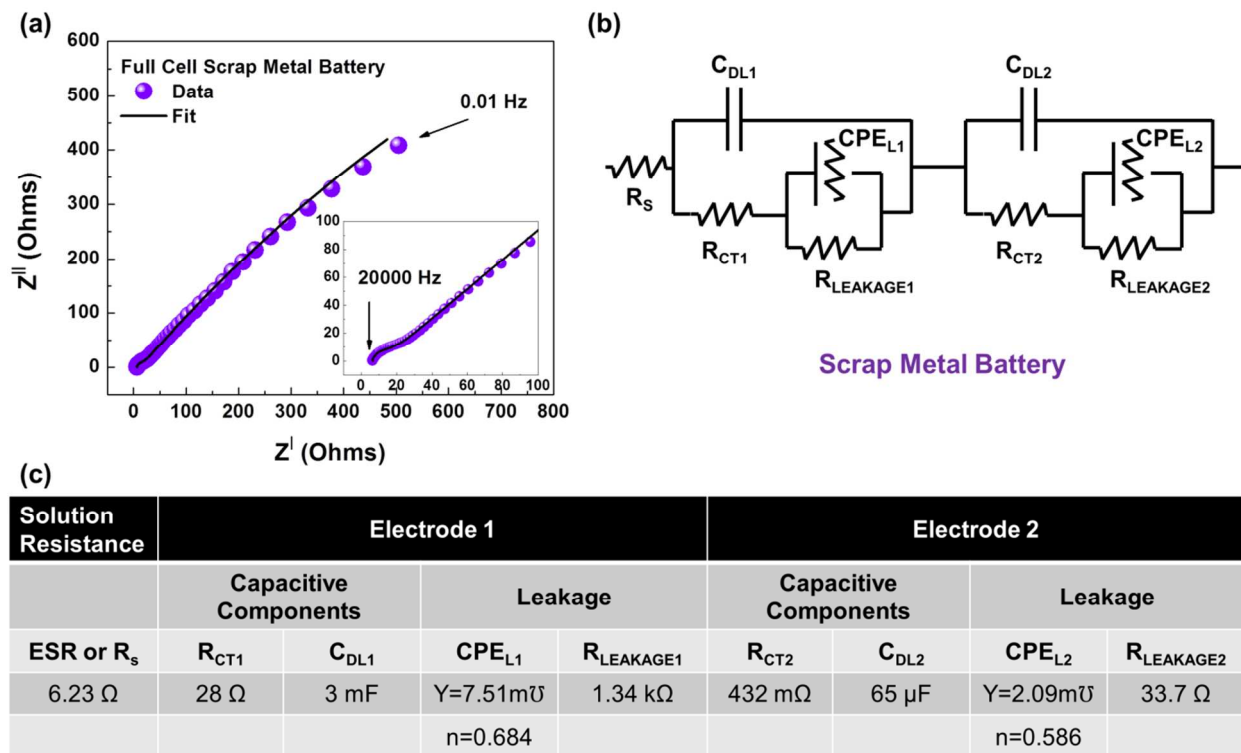


Figure S5. (a) Electrochemical impedance spectroscopy (Nyquist plot) of the scrap metal battery – full cell, (b) Equivalent circuit of the response of the scrap metal battery and (c) Fitting parameters for the full cell comprising of two electrodes (anodized steel and brass) of the scrap metal battery.

EIS measurements were performed in a full cell configuration to infer the equivalent series resistance (ESR) and charge transfer resistances (R_{CT}) of the scrap metal battery. Figure S5 (a) gives the Nyquist plot comprising of the real (x-axis) and imaginary components of impedance (y-axis) of the response of the scrap metal battery. The obtained response was fitted to a model typically applied for redox electrodes (Figure S5 (b)).¹⁶ Considering the fact that in our case, the system consists of a steel anode and brass cathode, the redox electrodes can be modeled identically and in a full cell configuration separated by the solution resistance R_S . From

the Nyquist plots, ESR values were estimated from the intercept of the curve with x-axis corresponding to a value of 6.23 Ω . For the scrap metal battery, the response of both electrodes was modeled using C_{DL} , R_{CT} , CPE_L and R_L which are all in series with the R_S or ESR and the fitting parameters are shown in Figure S5 (c). The high frequency regime gives the ESR of the system arising from electronic resistances. The charge transfer resistances and C_{DL} lie in the high to mid frequency region where the double layer component arises from the nanostructured nature of these electrodes. In the low frequency region, both the electrodes (anodized steel and brass) were modeled to have leakage capacitance and resistance associated with them represented by CPE_L and R_L respectively. The association of the resistive element R_L with CPE_L suggests a deviation from ideal behavior at low frequencies. As the electrodes used in this case are scrap metals which have a considerable amount of impurities, the effective energy storage capabilities are not that expected from ideal cases where ultrapure materials are used. Further purification steps prior to anodization treatment and optimizing the process parameters can further improve the performance of this scrap metal battery.

Recycling steps and their feasibility for battery processing

Recycling Process	Potential for Battery Processing
Collection	
Separation	Small items – direct anodization into a battery architecture
Shearing	
Shredding	Large items - could be anodized into a battery architecture after this step
Melting	
Purification	(could possibly skip this step for battery architectures)
Casting	All items - Could be cast into optimal architecture for battery performance

Table S6. A table showing the steps in the recycling process on the left, and the potential for the development of scrap metal into batteries after various steps in the process.

Commercially available common chemicals for scrap metal battery fabrication

Chemicals Used	Availability	Concentration	Cost
Hydrochloric Acid HCl (diluted from 37%)	Muriatic acid (Cleaning acid, used for cleaning mold, clearing clogged drains)	~31.5%	\$6 /liter (Walmart)
Potassium Hydroxide KOH (1-2M)	Commercially available in the form of flakes for liquid soap making	Caustic	\$3 /lb (Amazon)
Ammonium Fluoride NH₄F (0.05M)	For preventing fermentation, antiseptic agent	Reagent grade (available for moth proofing applications too as well as brewing malts)	\$33 /400g (eBay)
Ethylene Glycol	Antifreeze agent	Commercial grades for using in automobiles	\$9 /Gal (Walmart)

Table S7. Commercially available common chemicals that can be potentially used to develop the scrap metal battery system

REFERENCES

- (1) Futaba, D. N.; Hata, K.; Yamada, T.; Hiraoka, T.; Hayamizu, Y.; Kakudate, Y.; Tanaike, O.; Hatori, H.; Yumura, M.; Iijima, S., Shape-engineerable and highly densely packed single-walled carbon nanotubes and their application as super-capacitor electrodes. *Nat. Mater.* **2006**, *5*, 987-994.
- (2) Simon, P.; Gogotsi, Y., Materials for electrochemical capacitors. *Nat. Mater.* **2008**, *7*, 845-854.
- (3) Yu, G.; Hu, L.; Liu, N.; Wang, H.; Vosgueritchian, M.; Yang, Y.; Cui, Y.; Bao, Z., Enhancing the supercapacitor performance of graphene/MnO₂ nanostructured electrodes by conductive wrapping. *Nano Lett.* **2011**, *11*, 4438-4442.
- (4) Park, B.-O.; Lokhande, C.; Park, H.-S.; Jung, K.-D.; Joo, O.-S., Performance of supercapacitor with electrodeposited ruthenium oxide film electrodes—effect of film thickness. *J. Power Sources* **2004**, *134*, 148-152.
- (5) Feng, L.; Zhu, Y.; Ding, H.; Ni, C., Recent progress in nickel based materials for high performance pseudocapacitor electrodes. *J. Power Sources* **2014**, *267*, 430-444.
- (6) Wang, H.; Liang, Y.; Gong, M.; Li, Y.; Chang, W.; Mefford, T.; Zhou, J.; Wang, J.; Regier, T.; Wei, F., An Ultrafast Nickel–Iron Battery from Strongly Coupled Inorganic Nanoparticle/Nanocarbon Hybrid Materials. *Nat. Commun.* **2012**, *3*, 917.
- (7) Rakhi, R.; Chen, W.; Cha, D.; Alshareef, H. N., Substrate dependent self-organization of mesoporous cobalt oxide nanowires with remarkable pseudocapacitance. *Nano Lett.* **2012**, *12*, 2559-2567.
- (8) Higashi, S.; Lee, S. W.; Lee, J. S.; Takechi, K.; Cui, Y., Avoiding short circuits from zinc metal dendrites in anode by backside-plating configuration. *Nat. Commun.* **2016**, *7*, 11801.
- (9) Palacin, M. R., Recent advances in rechargeable battery materials: a chemist's perspective. *Chem. Soc. Rev.* **2009**, *38*, 2565-2575.
- (10) Majeau-Bettez, G.; Hawkins, T. R.; Strømman, A. H., Life cycle environmental assessment of lithium-ion and nickel metal hydride batteries for plug-in hybrid and battery electric vehicles. *Environ. Sci. Technol.* **2011**, *45*, 4548-4554.
- (11) Marom, R.; Amalraj, S. F.; Leifer, N.; Jacob, D.; Aurbach, D., A review of advanced and practical lithium battery materials. *J. Mater. Chem.* **2011**, *21*, 9938-9954.

- (12) Tarascon, J.-M.; Armand, M., Issues and challenges facing rechargeable lithium batteries. *Nature* **2001**, *414*, 359-367.
- (13) Conway, B. E., *Electrochemical supercapacitors: scientific fundamentals and technological applications*. Springer Science & Business Media: **2013**.
- (14) Simon, P.; Gogotsi, Y.; Dunn, B., Where do batteries end and supercapacitors begin? *Science* **2014**, *343*, 1210-1211.
- (15) Brousse, T.; Bélanger, D.; Long, J. W., To be or not to be pseudocapacitive? *J. Electrochem. Soc.* **2015**, *162*, A5185-A5189.
- (16) Barzegar, F.; Bello, A.; Momodu, D.; Dangbegnon, J.; Taghizadeh, F.; Madito, M.; Masikhwa, T.; Manyala, N., Asymmetric supercapacitor based on an α -MoO₃ cathode and porous activated carbon anode materials. *RSC Adv.* **2015**, *5*, 37462-37468.